The Feynman LECTURES ON PHYSICS Vol. I (1963)

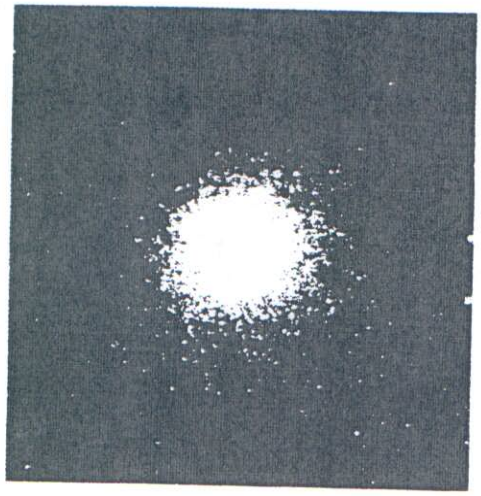

Fig. 7–8. A globular star cluster.

That the law of gravitation is true at even bigger distances is indicated in Fig. 7–8. If one cannot see gravitation acting here, he has no soul. This figure shows one of the most beautiful things in the sky—a globular star cluster. All of the dots are stars. Although they look as if they are packed solid toward the center, that is due to the fallibility of our instruments. Actually, the distances between even the centermost stars are very great and they very rarely collide. There are more stars in the interior than farther out, and as we move outward there are fewer and fewer. It is obvious that there is an attraction among these stars. It is clear that gravitation exists at these enormous dimensions, perhaps 100,000 times the size of the solar system. Let us now go further, and look at an *entire galaxy*, shown in Fig. 7–9. The shape of this galaxy indicates an obvious tendency for its matter to agglomerate. Of course we cannot prove that the law here is precisely inverse square, only that there is still an attraction, at this enormous dimension, that holds the whole thing together. One may say, "Well, that is all very clever but why is it not just a ball?" Because it is *spinning* and has *angular momentum* which it cannot give up as it contracts; it must contract mostly in a plane. (Incidentally, if you are looking for a good problem, the exact details of how the arms are formed and what determines the shapes of these galaxies has not been worked out.) It is, however, clear that the shape of the galaxy is due to gravitation even though the complexities of its structure have not yet allowed

Fig. 7–9. A galaxy.

e e

$\frac{F_{grav}}{F_{ee}} \approx 2.5 \times 10^{-43}$

LO SPETTRO ELETTROMAGNETICO

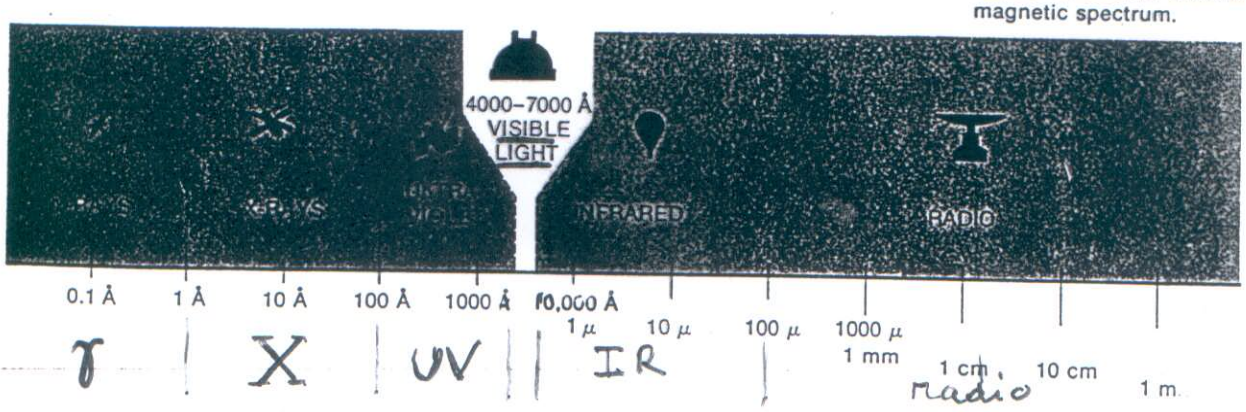

Figure 2–7 The electromagnetic spectrum.

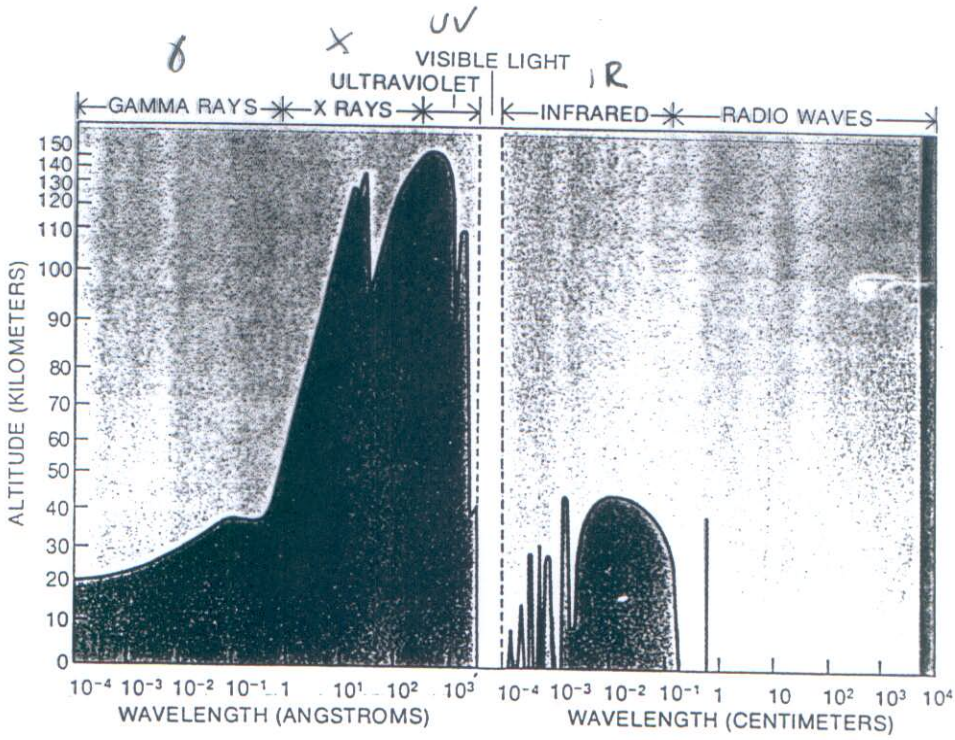

Figure 2–8. Windows of transparency in the terrestrial atmosphere allow only part of the solar spectrum to penetrate to the earth's surface. The curve specifies the altitude where the intensity of arriving radiation is reduced to half its original value. When the curve touches the lower axis (as it does, for example, between 1 cm and 10^3 cm), the atmosphere is completely transparent.

(Pasachoff & Kutner 1978)

ATOMO DI IDROGENO

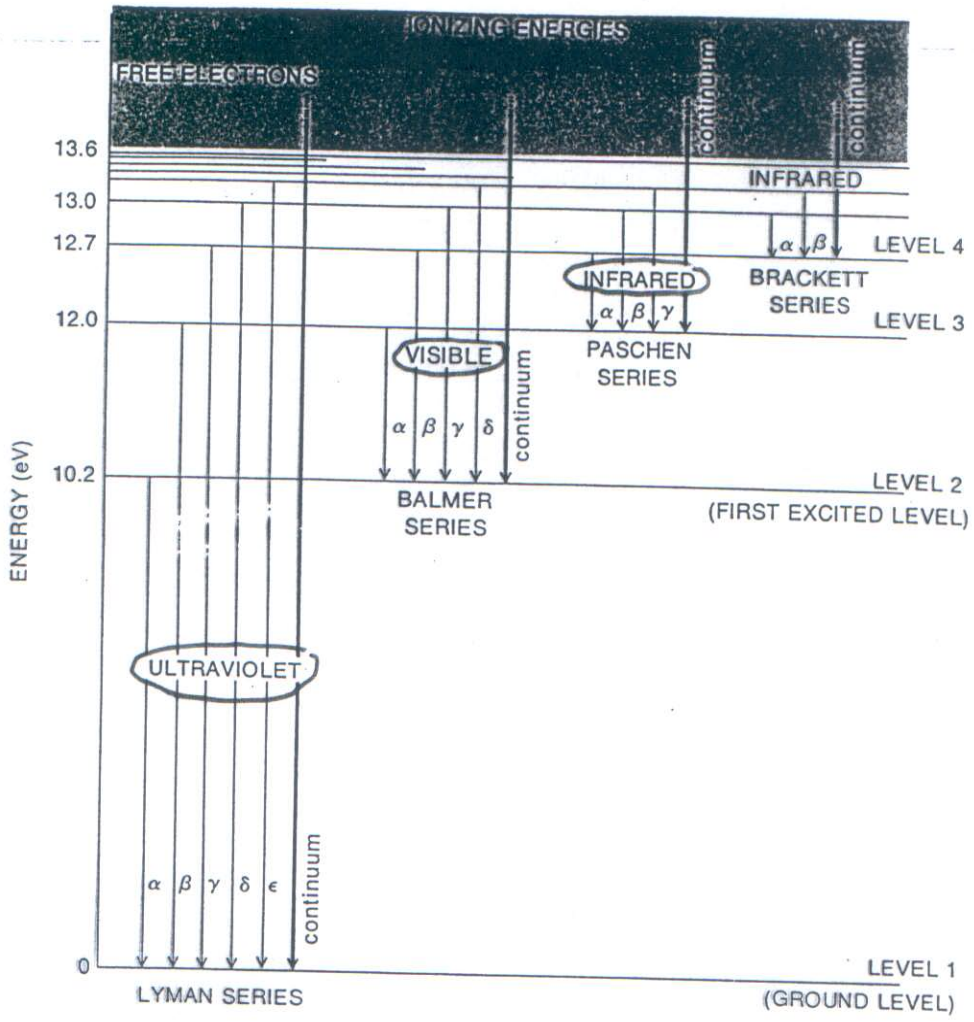

Figure 2–29 The energy levels of hydrogen and the series of transitions among the lowest of these levels.

Lyα 1216 Å

BALMER

$1\,eV = 1.6 \times 10^{-12}$ erg

$\lambda(1\,eV) = 12,398.\text{Å} = 1.2398 \times 10^{-4}$ cm $= 1.2398\,\mu$

(4

T Treu 2000
Ph.D. Thesis

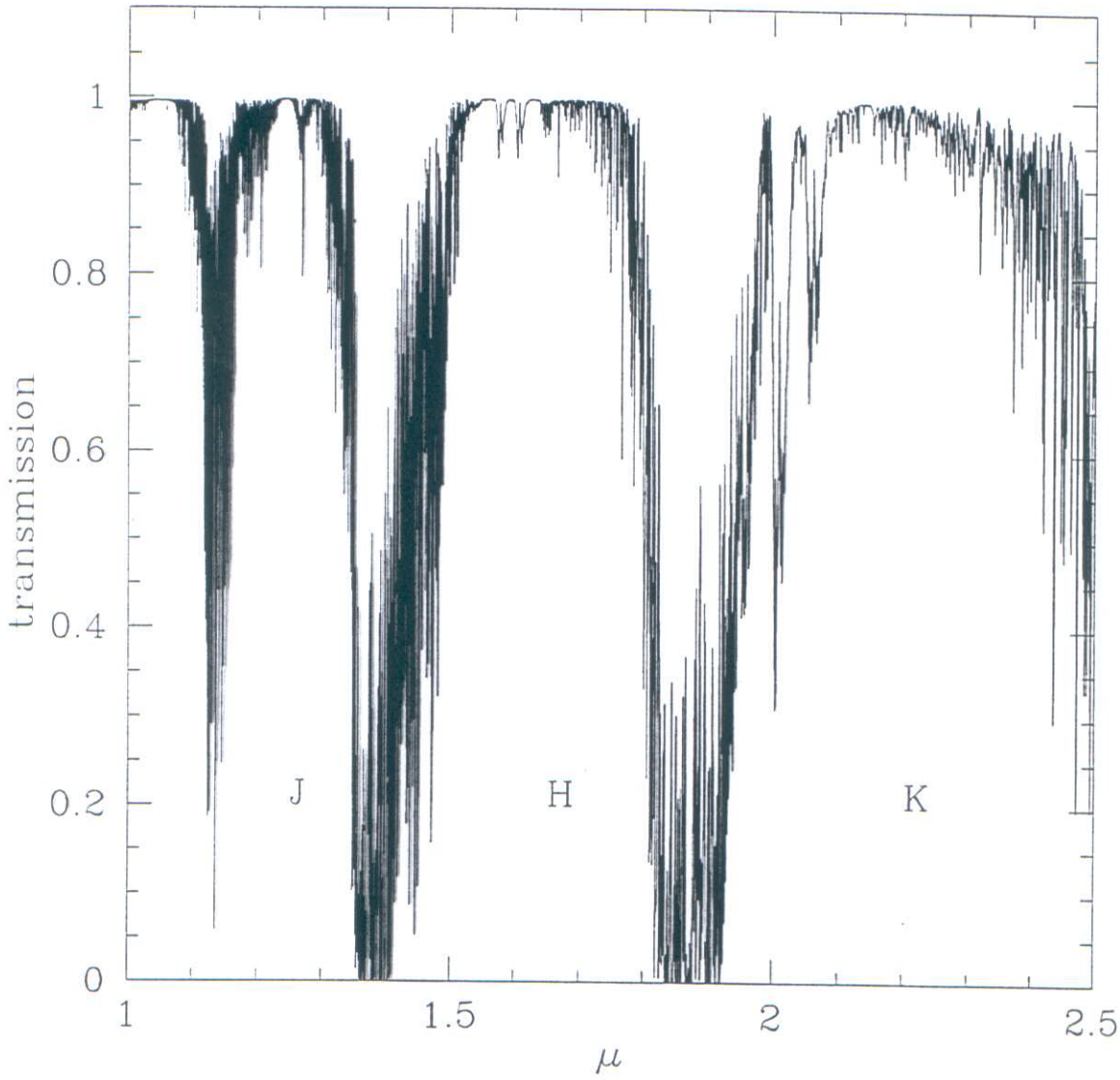

Figure 1.2: Atmospheric transmission at Mauna Kea, Hawaii (USA), one of the best sites in the world. The standard IR filters (J, H, and K; see Appendix B) are located in correspondence with the principal transmission windows.

(formerly NGST) (5)

JAMES WEBB SPACE TELESCOPE

The First Light Machine

JWST Fast Facts

The James Webb Space Telescope (JWST) is an orbiting infrared observatory that will take the place of the Hubble Space Telescope at the end of this decade. It will study the Universe at the important but previously unobserved epoch of galaxy formation. It will peer through dust to witness the birth of stars and planetary systems similar to our own. And using JWST, scientists hope to get a better understanding of the intriguing dark matter problem. The JWST is also a key element in NASA's Origins Program.

Proposed Launch Date:	August 2011 → moved to 2013
Proposed Launch Vehicle:	Ariane 5
Mission Duration:	5 - 10 years
Total payload mass:	Approx 6200 kg, including observatory, on-orbit consumables and launch vehicle adaptor.
Diameter of primary Mirror:	~6.5 m (21.3 ft) ✓
Clear aperture of primary Mirror:	25 m^2
Primary mirror material:	beryllium
Mass of primary mirror:	about one-third as much as Hubble's
Focal length:	TBD
Number of primary mirror segments:	18
Optical resolution:	~0.1 arc-seconds
Wavelength coverage:	0.6 - 28 microns
Size of sun shield:	~22 m x 10 m (72 ft x 33 ft)
Orbit:	1.5 million km from Earth at L2 Point ✓
Operating Temperature:	<50 K (-370 °F)
→ **Cost:**	$824.8 million ?

http://www.stsci.edu/resources/

Cosmology & galaxy evolution
dark matter
formation of stars & planets

Monday, 05-Jan-2004

Massimo Stiavelli
Sciana Working Group
"Interdisciplinary Scientist"

ALMA

The Atacama Large Millimeter/submillimeter Array www.eso.org/sci/facilities/alma

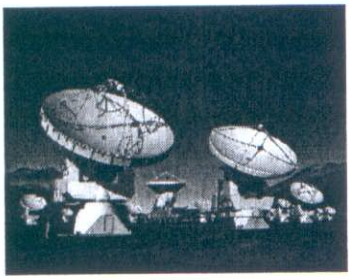

The Atacama Large Millimeter/submillimeter Array (ALMA), one of the largest ground-based astronomy projects of the next decade, is a major new facility for world astronomy. ALMA will be comprised of a giant array of 12-m submillimetre quality antennas, with baselines of several kilometres. An additional, compact array of 7-m and 12-m antennas is also foreseen. Construction of ALMA started in 2003 and will be completed in 2012. The ALMA project is an international collaboration between Europe, Japan and North America in cooperation with the Republic of Chile.

(5bis

up to 80 antennas at 5000 m above sea level 0.3–9.6 mm

baselines 15m → 18km resolution (best) 0.005"

more about ALMA

ELT

ESO
European Organisation for Astronomical Research in the Southern Hemisphere

The European ELT

diameter : 42 m

expected operations: 2018

Science Users Information > Future Facilities > E-ELT

24 Feb 2009

www.eso.org/sci/facilities/eelt/

THE EUROPEAN EXTREMELY LARGE TELESCOPE ("E-ELT") PROJECT

GAIA

Mission Home
- Summary
- Fact Sheet
- Objectives
- Mission Team

News

Mission Science
- Galactic Structure
- Stars
- Solar System
- Extra-solar Planets

Spacecraft
- Payload Module
- Service Module

Mission

GAIA

Make this your homepage http://gaia.esa.int 24-Feb-2009 09:2

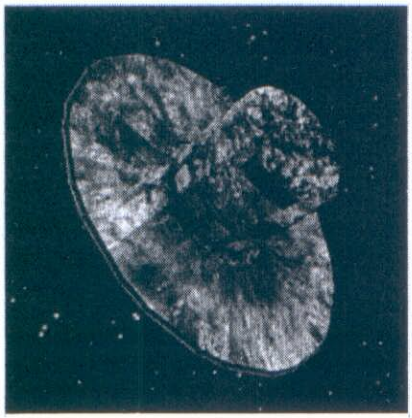

IMAGES AND VIDEOS

LAUNCH DATE:	Dec-2011
MISSION END:	2020
LAUNCH VEHICLE:	Soyuz-Fregat
LAUNCH MASS:	2030 kg
MISSION PHASE:	Implementation

ORBIT:
Lissajous-type orbit around L2

astrometric accuracy 20 μas

OBJECTIVES:
To create the largest and most precise three dimensional chart c Galaxy by providing unprecedented positional and radial velocity measurements for about one billion stars in our Galaxy and throughout the Local Group.

SKA

- SKA science
- FAQ

QUICK LINKS
- News & meetings
- Documents & presentations
- Timeline
- Location & design
- Pictures & movies
- Partners & Links
- Contacts
- Site map

2012 SKA site selection

2016-21 construction of full array

The Square Kilometre Array (SKA) will probe the gaseous component of the early Universe, thereby addressing fundamental questions in research on the origin and evolution of the Universe. The SKA will complement planned facilities at other wavelengths, such as ALMA and James Webb Space Telescope (JWST). HI, CO and continuum radiation would be observed from the interstellar medium of most of the galaxies the JWST will discover in the infrared at large redshifts.

www.skatelescope.org

Credit: Canadian glacti

Extensive discussion of the science drivers and of the evolving technical possibilities has led to a concept for the Square Kilometre Array and a set of design goals. The SKA will be an interferometric array of individual antenna stations, synthesizing an aperture with diameter of up to several 1000 kilometers. A number of configurations are under consideration to distribute the 1 million square metres of collecting area. These include 30 stations each with the collecting area equivalent to a 200 metres diameter telescope, and 150 stations each with the collecting area of a 90 telescope (more about design and location proposals).

Approximately 50% of the collecting area is to be contained within a centrally-condensed inner array 5km diameter to provide ultrahigh brightness sensitivity at arc-second scale resolution for studies of t faint spectral line signatures of structures in the early Universe. Another 25 % of the collecting area w located within a diameter of 150 km, and the remainder out to 3000 km or more. This high angular resolution capability will allow imaging of faint emission from the interstellar medium of distant galaxi well as the surface of stars, and the active nuclei of galaxies.

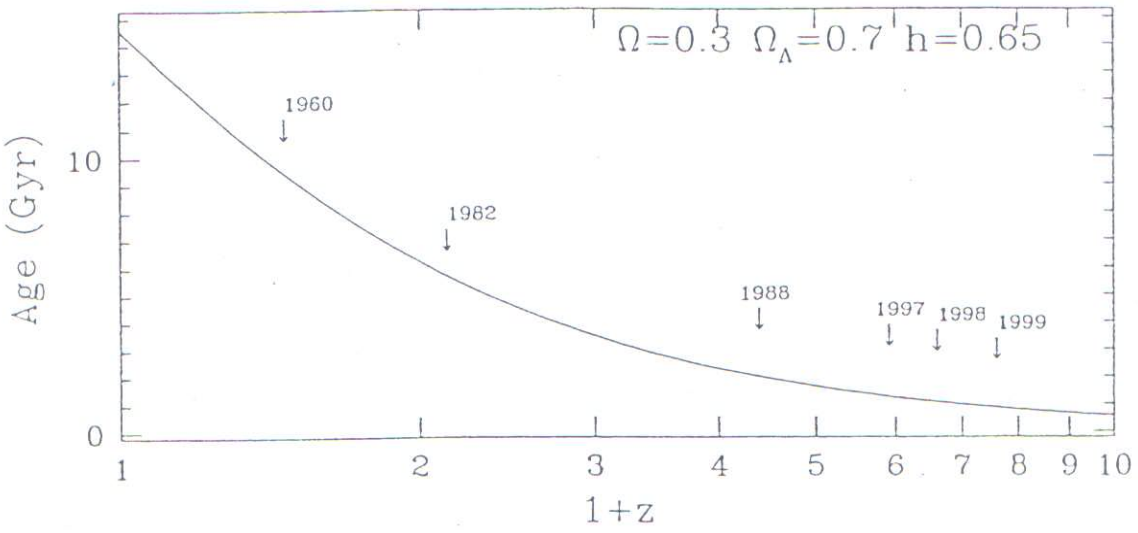

Figure 1.1: Age of the Universe for two sets of values of the cosmological parameters, matter density (Ω), cosmological constant (Ω_Λ), and Hubble constant (h), defined as in Chapter 2. The redshift of the most distant galaxy known is indicated by an arrow labeled with the year of publication. Until 1997 the galaxies are radio selected. Redshifts are taken from Minkowski (1960), Spinrad (1982), Chambers et al. (1988), Franx et al. (1997), Weynmann et al. (1998), Chen et al. (1999).

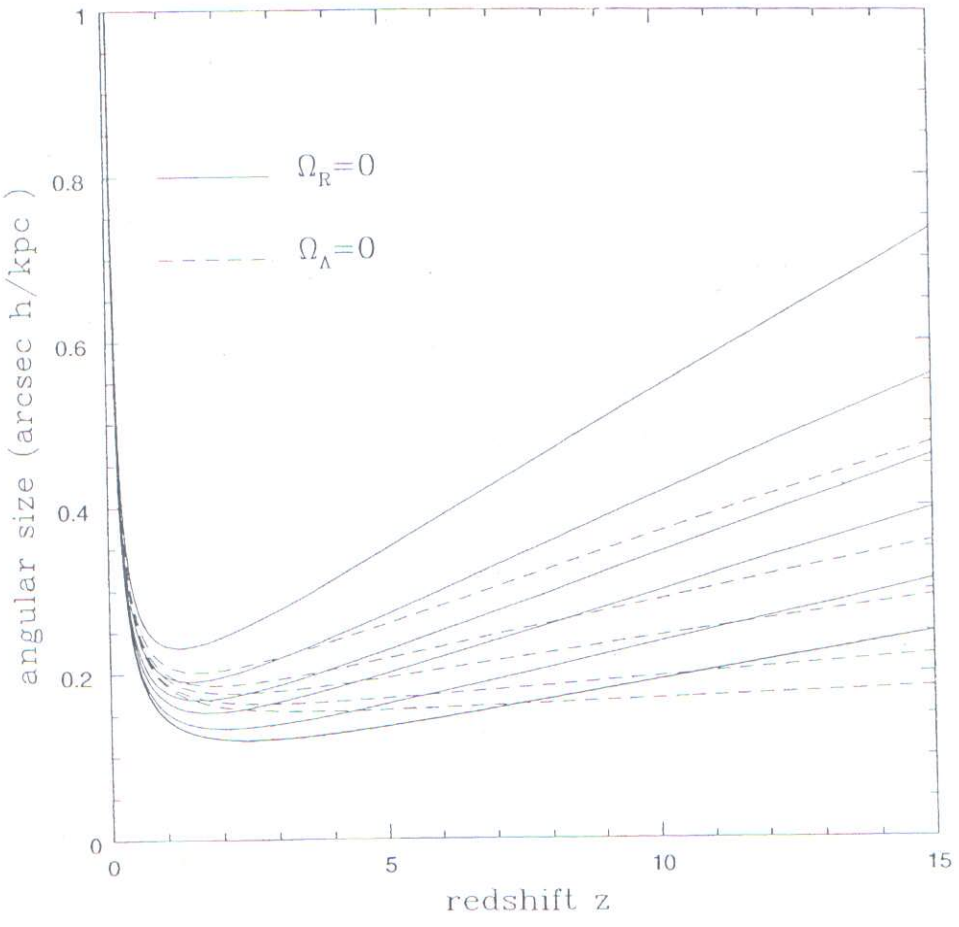

Fig. 25.5. Angular size as a function of redshift for different values of the density parameter Ω (from bottom to top: $\Omega = 0.05, 0.1, 0.2, 0.3, 0.5, 1$); solid and dashed curves are as in Fig. 25.4. The quantity h is the reduced Hubble constant.

La radiazione di fondo cosmico: A.A. Penzias & R.W. Wilson (1965)

7

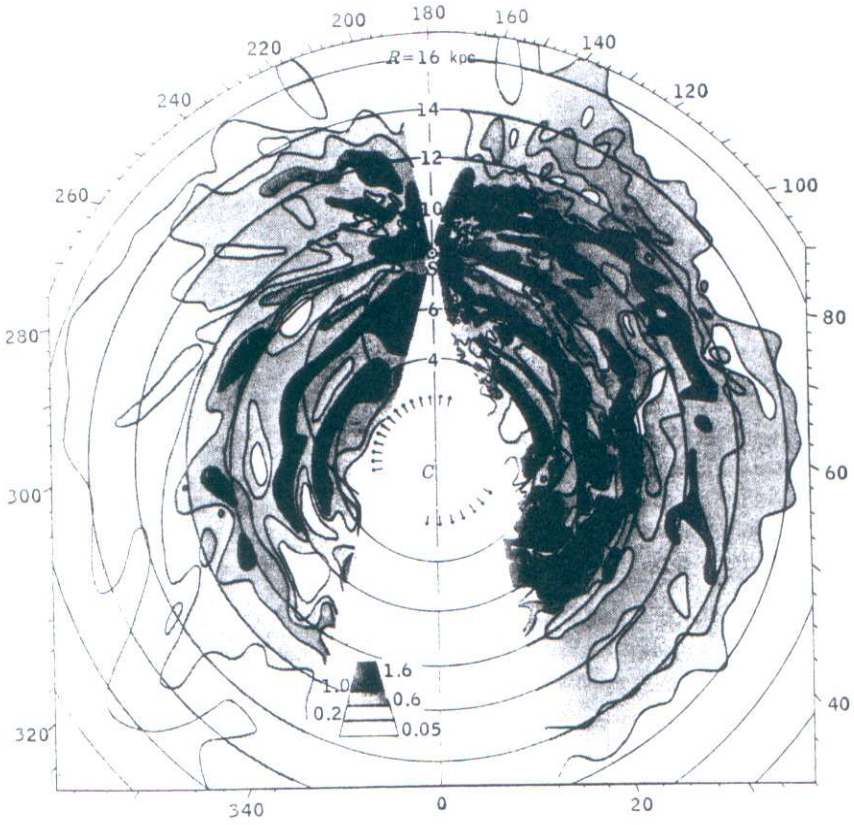

21cm

van de Hulst (1945)

Ewen & Purcell (1951)

Figure 6.1
Distribution of hydrogen in the galactic plane; the density scale is in atoms/cm^3 [32, 31].

Oort, Kerr, Westerhout 1958

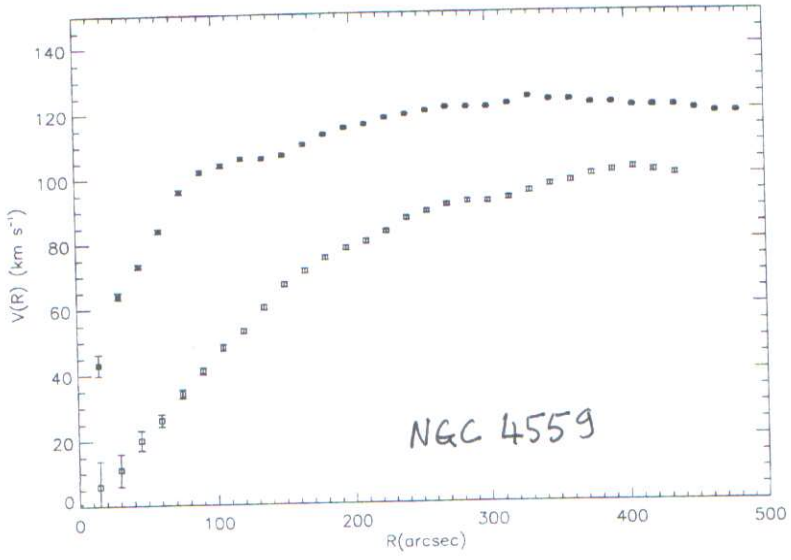

21cm

Figura 4.6: Curva di rotazione del gas anomalo (quadrati vuoti) e curva di rotazione del disco freddo (quadrati pieni).

Claudia V. Barbieri, Tesi di Laurea 2004, Un. Milano

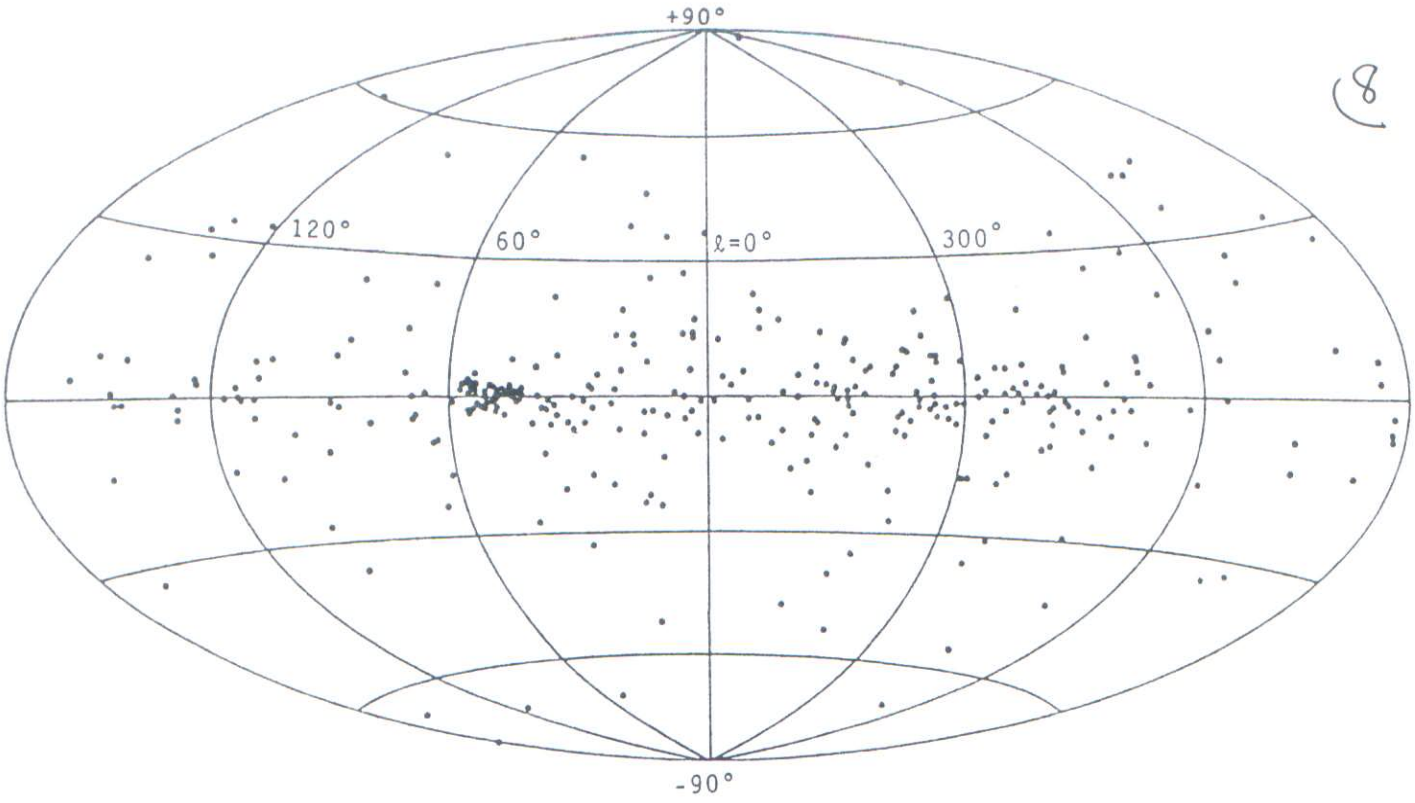

FIG. 1.2. Galactic distribution of pulsars. The location of 330 pulsars in galactic coordinates. Galactic center is in middle, with galactic latitude (unlabeled except at poles) in 30° increments. The dense cluster near 60° longitude represents the high sensitivity (but limited coverage) of the Arecibo telescope. From *Pulsars*, by R. N. Manchester and J. H. Taylor. Copyright © 1977 by W. H. Freeman and Company. Reprinted by permission.

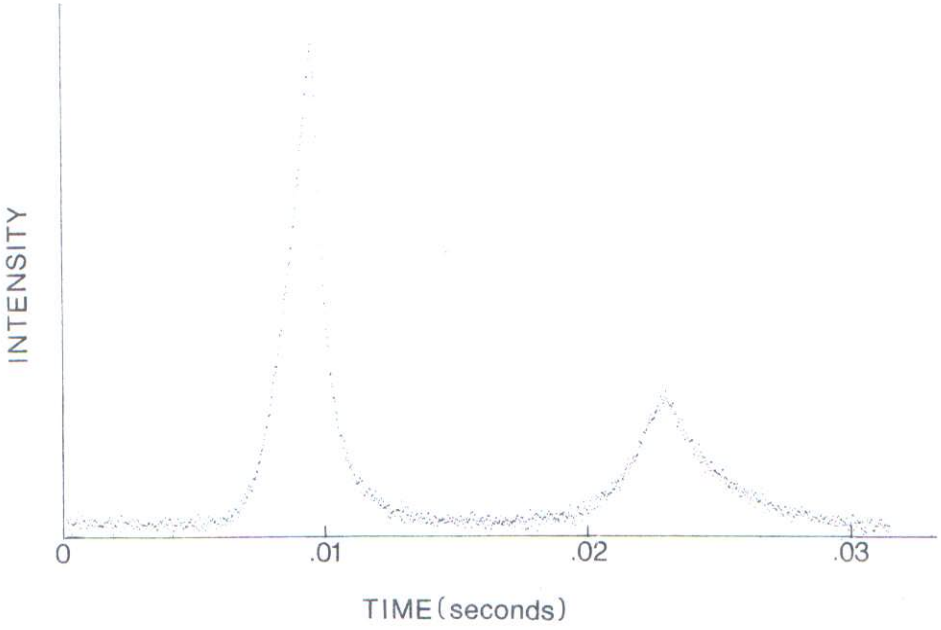

Figure 11–13 Some pulsars have not only a main pulse but also a subsidiary pulse called an *interpulse*. The pulse shown here is the result of averaging many pulses from the pulsar in the Crab Nebula, NP 0532, observed in visible light. Its period is 0.033 sec.

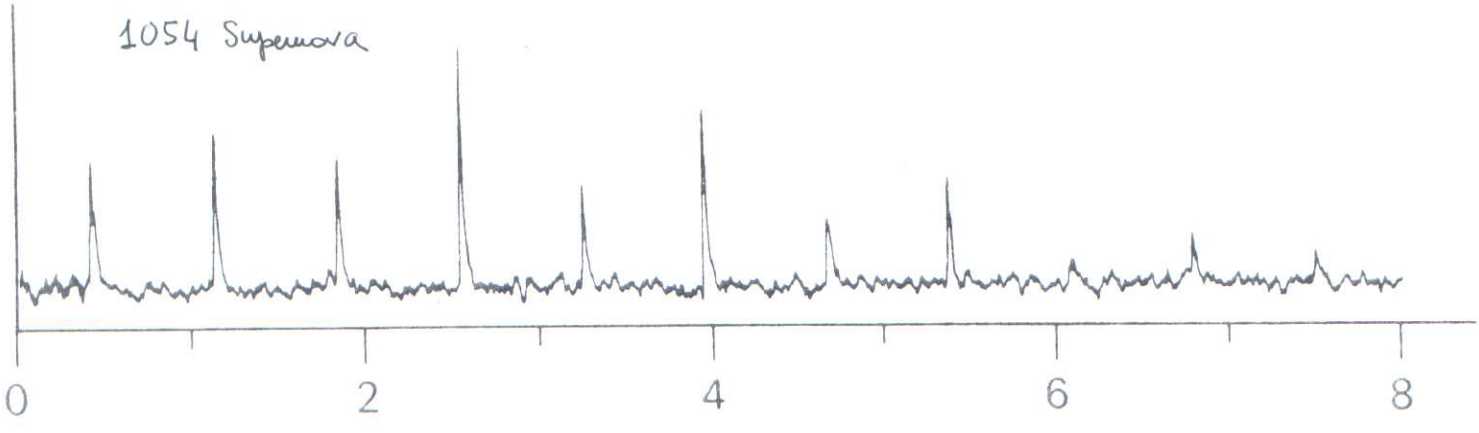

FIG. 1.1. Pulse train. Chart record of individual pulses from the 0.714 s pulsar PSR 0329 + 54 at 410 MHz. From *Pulsars*, by R. N. Manchester and J. H. Taylor. Copyright © 1977 by W. H. Freeman and Company. Reprinted by permission.

TABLE 1.1 Some Important Pulsars

Designation	Popular Name	Notable Feature(s)
0531 + 21	Crab pulsar (NP 0532) (NP 0531)	Fastest known for many years (.033 s) pulsed emission from radio to γ-ray obvious supernova association giant pulses glitches variations in dispersion measure extremely "inefficient" (10^{-9} of spin-down energy converted to radio-emission)
0540 − 693	LMC pulsar	Very similar to Crab pulsar, but no glitches! 55 kpc away in LMC pulsed optical
0833 − 45	Vela pulsar	Supernova association glitches pulsed optical and γ-ray
1913 + 16	Hulse-Taylor binary	First binary pulsar discovered evidence of gravitational radiation consistent with general relativity
1937 + 214	Millisecond pulsar	Fastest known: 642 rotations/s
1957 + 20	Eclipsing pulsar	Second fastest millisecond pulsar eclipsed by 0.02 $M_\odot$ companion every 9.2 hours
1951 + 32	CTB 80 Pulsar	Pulsar inside a wind-blown (?) shell
1845 − 19	—	Presently slowest known: 4.3082 s period
1237 + 25	—	Exceptionally complicated pulse shape (5 components)
1641 − 45	—	Slow pulsar also having glitches
0809 + 74	—	Both nulls and drifts
0826 − 34	—	Exceptionally wide pulse profile (≈ 145°) numerous subpulses drifting back and forth
1919 + 21	CP 1919	First pulsar discovered (CP = Cambridge pulsar, a largely discontinued designation)
1821 − 24	Pulsar in M28	First pulsar discovered in a globular cluster also a millisecond pulsar

(1969)

(1974)

T ≈ 1.337s

(1967; J. Bell, A. Hewish)

(1987; Lyne et al.)

da F.C. Michel (1991) Theory of Neutron Star Magnetospheres

!

Most of the known pulsars (141) in globular clusters (26 clusters) have spin frequency in the range 10^2–10^3 Hz, i.e. they are millisecond pulsars!

(Jan. 2009)

Paolo D'Avanzo,
Tesi di Laurea 2003,
Un. Milano

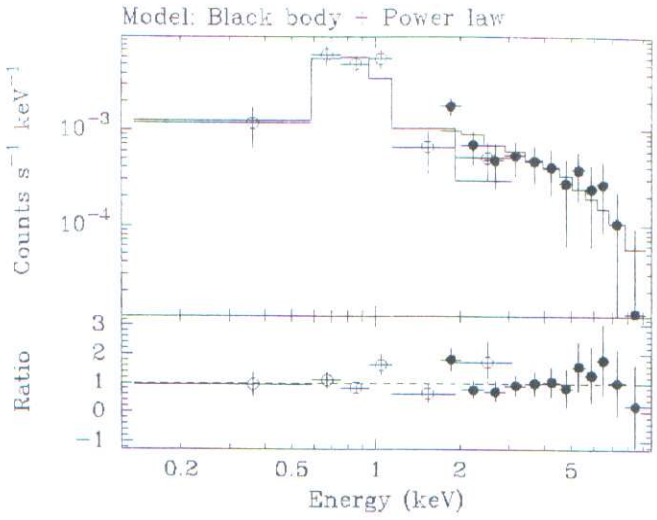

$T \sim 15.1$ hr
neutron star ($M \sim 1.4 M_\odot$?)
+
K dwarf/subgiant
($M < 1 M_\odot$)

Figura 2.3: Spettro di Cen X-4 in quiescenza ottenuto con gli strumenti LECS (cerchi) e MECS (punti) montati sul satellite *BeppoSAX*. Lo spettro è confrontato con un profilo di corpo nero sommato a legge di potenza. Nel pannello inferiore è indicato il rapporto tra i dati ed il modello presentato (da Campana et al. 2000).

Prima sorgente extra-solare X: Sco X-1; B. Rossi, R. Giacconi ..... (1962)
$\leftrightarrow$ QPOs

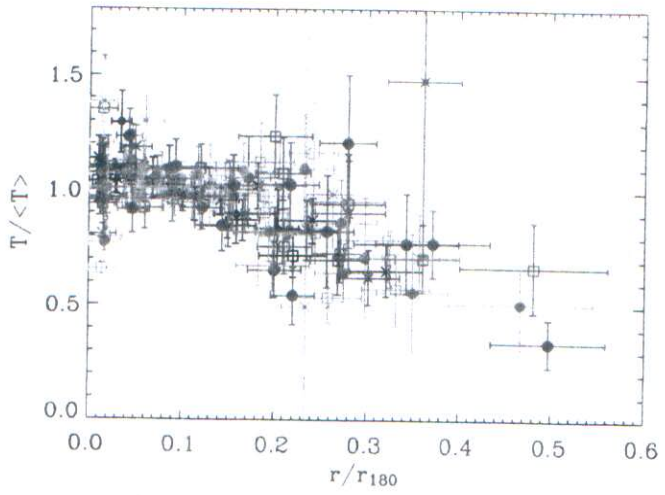

Alberto Leccardi
Tesi di Laurea 2005,
Un. Milano

Figura 1: *Profilo di temperatura di un campione di 21 ammassi di galassie misurato, nel corso di questa Tesi, a partire da dati raccolti dal satellite* XMM-Newton. *I raggi sono espressi in unità di* r_{180} ($r_{180} \simeq r_{vir}$) *e le temperature sono normalizzate alla temperatura media di ciascun ammasso tra* $0.05\ r_{180}$ *e* $0.20\ r_{180}$. *Ammassi diversi sono indicati con simboli e colori differenti.*

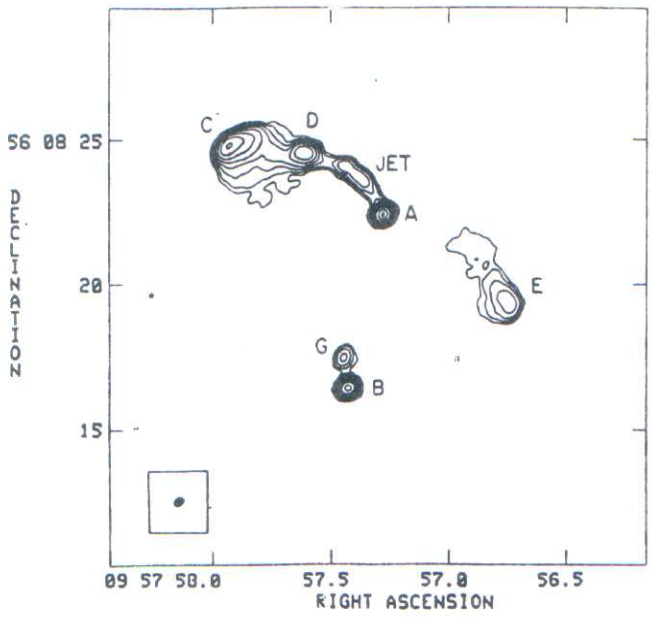

Fig. 2.6. VLA 6-cm map of 0957+561 (courtesy of D. Roberts)

QSO : $z \simeq 1.4$, 2 immagini A, B separate da 6"

galassia-lente : $z_d \approx 0.36$

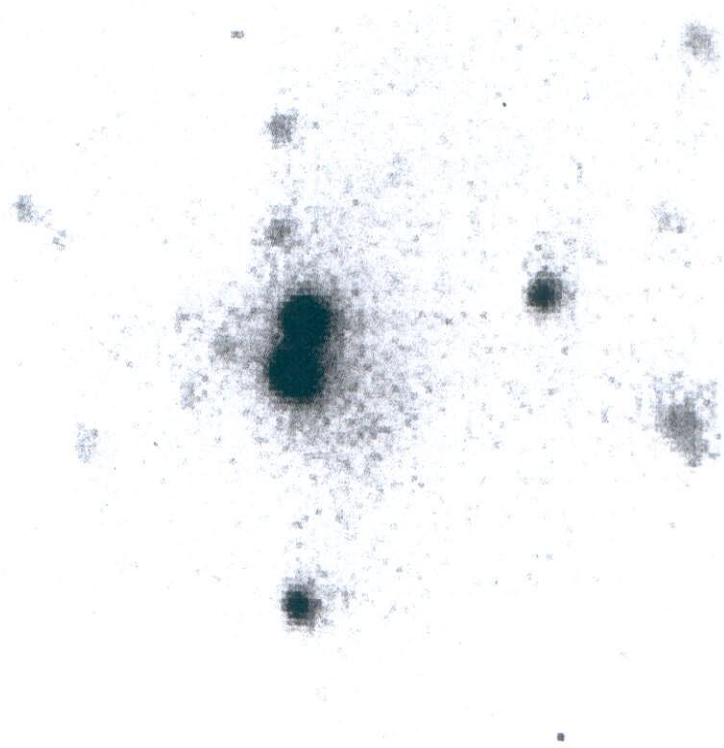

Fig. 2.5. Optical view of 0957+561 (courtesy of R. Schild)

(see Walsh, Carswell, Weymann 1979)

Igor Proverbio, Tesi di Laurea 2004, Un. Milano

Satellite	Tempo di vita	Strumento	Intervallo energetico	Campo di vista
IL PASSATO				
Vela-5B	23 mag 69 - 19 giu 79		**3-750keV**	
		All-Sky Monitor	3-12keV	$6.1^\circ \times 6.1^\circ$
		γ-Ray detector	150-750keV	
COS-B	9 ago 75 - 25 apr 82		**2keV-5GeV**	
		γ-Ray detectors	30MeV-5GeV	
		prop-counters	2-12keV	
Ginga	5 feb 87 - 1 nov 91		**1-500keV**	
		All-Sky Monitor	1-20keV	$1^\circ \times 180^\circ$
		GRB detectors	1.5-500keV	tutto il cielo
Granat	1 dic 89 - 27 nov 98		**2keV-100MeV**	
		SIGMA	0.03-1.3 MeV	$11.4^\circ \times 10.5^\circ$
		WATCH	6-120keV	tutto il cielo
		PHEBUS	0.1-500MeV	tutto il cielo
		KONUS-B	0.02-8MeV	tutto il cielo
		TOURNESOL	0.002-20MeV	$5^\circ \times 5^\circ$
CGRO	5 apr 91 - 4 giu 00		**30keV-30GeV**	
		BATSE	20-1000keV	tutto il cielo
		OSSE	0.05-10MeV	
		Comptel	0.8-30MeV	1sr
		EGRET	30 MeV-10GeV	
BeppoSAX	30 apr 96 - 30 apr 02		**0.1-300keV**	
		NFI	0.1-300keV	1sr
		WFC	2-30keV	$40^\circ \times 40^\circ$
IL PRESENTE				
RXTE	30 dic 95 - ora		**2-250keV**	
		PCA	2-60 keV	
		HEXTE	15-250keV	
		All-Sky Monitor	2-10 keV	tutto il cielo
Chandra	23 lug 99 - 5 anni		**0.1-10keV**	
		HRC	0.1-10keV	$30^\circ \times 30^\circ$
XMM	10 dic 99 - 10 anni		**0.1-15keV**	
		X-Ray instruments	0.1-15keV	
		Opt.Monitor	180-650nm	17'×17'
HETE-2	9 ott 00 - 2 anni		**0.5-400keV**	
		X-Ray detectors	0.5-25keV	
		γ-Ray detectors	6-400keV	3 sr
Integral	17 ott 02 - 10 anni		**15keV-10MeV**	
		JEM-X	3-35keV	$4.8^\circ \times 4.8^\circ$
		γ-Ray instruments	15keV-10MeV	$16^\circ \times 16^\circ$
IL FUTURO				
Swift	lancio nel 2004		**2eV-150keV**	
		BAT	15-150keV	2.0 sr
		XRT	0.2-10keV	$23.6^\circ \times 23.6^\circ$
		UVOT	170-650nm	17'×17'
Agile	lancio nel 2005		**30MeV-50GeV**	
		GRID	30MeV-50GeV	
		SuperAGILE	10-40keV	> 0.8 sr
GLAST	lancio nel 2006 / 2008		**20MeV-300GeV**	
		LAT	20 MeV-300GeV	> 2sr
		GBM	<10keV->25MeV	tutto il cielo

Tabella 1.1: Missioni spaziali per studio dei GRB.

interpretate come righe di annichilazione e^+e^- a 511keV spostate verso il rosso di circa il 20% per effetto del campo gravitazionale alla superficie di stelle di neutroni, (Murakami *et al.*, 1988 [89]); la teoria fu anche in parte confermata dall'associazione del resto di supernova della stella di neutroni N49 nella LMC con GRB 790305 (Evans *et al.*, 1988 [30]).

1967 (Vela)

1997 (BeppoSax)

Compton Gamma Ray Obs

"Fermi" ← GLAST

all sky survey

orbit 95' period

(1) first "gamma ray pulsar" T ~ 0,317s D ≈ 3kpc

(2) Most powerful gamma ray burst

look back time 12.2 10^9 yr

Sept 16 2008

per posizionare. 8 ore dopo il *trigger*, i NFI (*Narrow Field Instruments*), aventi una precisione dell'ordine dell'arcominuto nella localizzazione della sorgente X. Fu così possibile ottenere le prime immagini in X ad alta risoluzione dell'*afterglow* di GRB 970228 (Costa *et al.*, 1997 [22]). Furono quindi distribuite le coordinate per osservazioni con telescopi a terra e fu possibile ottenere la prima controparte ottica (van Paradijs *et al.*, 1997 [138]; si veda la Figura 1.2).

burst	Rivelazione (banda X)	O	R	Fluenza γ [erg/cm^2]	*redshift*	E_0 [erg]
GRB970228	BeppoSAX	+	-	1×10^{-5}	-	-
GRB970508	BeppoSAX	+	+	2×10^{-6}	0.835	2×10^{51}
GRB970616	BeppoSAX	-	-	4×10^{-5}	-	-
GRB970815	RXTE	-	-	1×10^{-5}	-	-
GRB970828	RXTE	-	-	7×10^{-5}	-	-
GRB971214	RXTE	+	+	1×10^{-5}	3.418	1×10^{53}
GRB971227	BeppoSAX	-	-	9×10^{-7}	-	-
GRB980326	BeppoSAX	-	-	1×10^{-6}	-	-
GRB980329	BeppoSAX	+	+	5×10^{-5}	-	-
GRB980425	BeppoSAX	+	+	4×10^{-6}	0.0085	7×10^{47}
GRB980515	BeppoSAX	-	-	1×10^{-6}	-	-
GRB980519	BeppoSAX	+	+	3×10^{-5}	-	-
GRB980703	RXTE	+	+	5×10^{-5}	0.966	1×10^{53}

Tabella 1.2: Dati osservativi di diversi GRB per cui è stato individuato l'*afterglow*. Le colonne O e R indicano se l'emissione è stata rivelata rispettivamente nell'ottico e nel radio. L'energia totale E_0 del *burst* è stata stimata attraverso l'integrale sul tempo dell'energia irradiata ed il *redshift* osservati, assumendo emissione sferica e un Universo piatto con parametri cosmologici definiti da $\Omega = 1$, $\Lambda = 0$, con $H_0 = 65$ km/sec/Mpc. Tratto da Piran, 1998 [105].

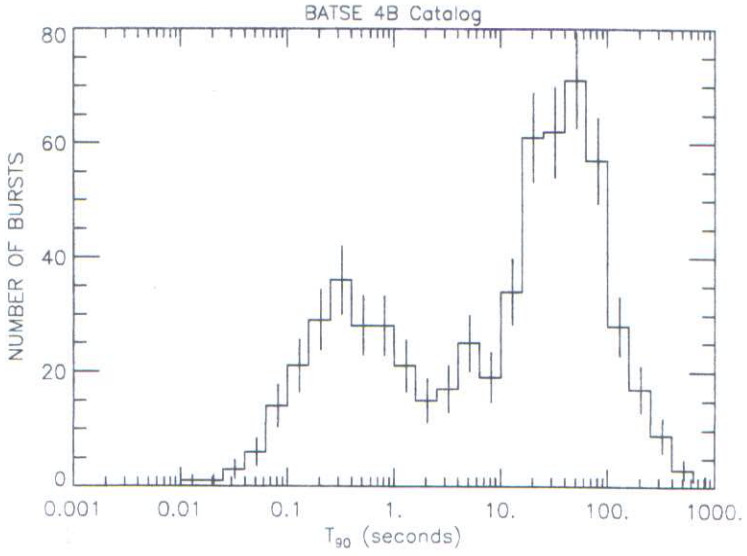

Figura 1.3: Distribuzione bimodale dei GRB. L'immagine, tratta dal Catalogo di BATSE, mostra la distribuzione dei *burst* in base al parametro di durata T_{90}.

von Helmholtz 1854 ; Lord Kelvin 1897 "Tempo di kelvin"
A. Eddington 1920 "reazioni nucleari"
R.H. Fowler 1926 ; S. Chandrasekhar 1931 "stelle nane bianche"
W. Baade & F. Zwicky 1934 ; J.R. Oppenheimer & G. Volkoff 1939 "stelle di neutroni"

$GM_\odot^2/(R_\odot L_\odot) \approx E_m/L_\odot \approx 10^7\,yr$

da J. N. Bahcall (1989) Neutrino Astrophysics

Table 1.1. The pp chain in the Sun. The average number of pp neutrinos produced per termination in the Sun is 1.85. For all other neutrino sources, the average number of neutrinos produced per termination is equal to (the termination percentage/100).

Reaction	Number	Termination† (%)	ν energy (MeV)
$p + p \rightarrow {}^2H + e^+ + \nu_e$	1*a*	100	≤ 0.420
or			
$p + e^- + p \rightarrow {}^2H + \nu_e$	1*b* (pep)	0.4	1.442
${}^2H + p \rightarrow {}^3He + \gamma$	2	100	
${}^3He + {}^3He \rightarrow \alpha + 2p$	3	85	
or			
${}^3He + {}^4He \rightarrow {}^7Be + \gamma$	4	15	
${}^7Be + e^- \rightarrow {}^7Li + \nu_e$	5	15	(90%) 0.861 (10%) 0.383
${}^7Li + p \rightarrow 2\alpha$	6	15	
or			
${}^7Be + p \rightarrow {}^8B + \gamma$	7	0.02	
${}^8B \rightarrow {}^8Be^* + e^+ + \nu_e$	8	0.02	< 15
${}^8Be^* \rightarrow 2\,\alpha$	9	0.02	
or			
${}^3He + p \rightarrow {}^4He + e^+ + \nu_e$	10 (hep)	0.00002	≤ 18.77

†The termination percentage is the fraction of terminations of the pp chain, $4p \rightarrow \alpha + 2e^+ + 2\nu_e$, in which each reaction occurs. The results are averaged over the model of the current Sun. Since in essentially all terminations at least one pp neutrino is produced and in a few terminations one pp and one pep neutrino are created, the total of pp and pep terminations exceeds 100%.

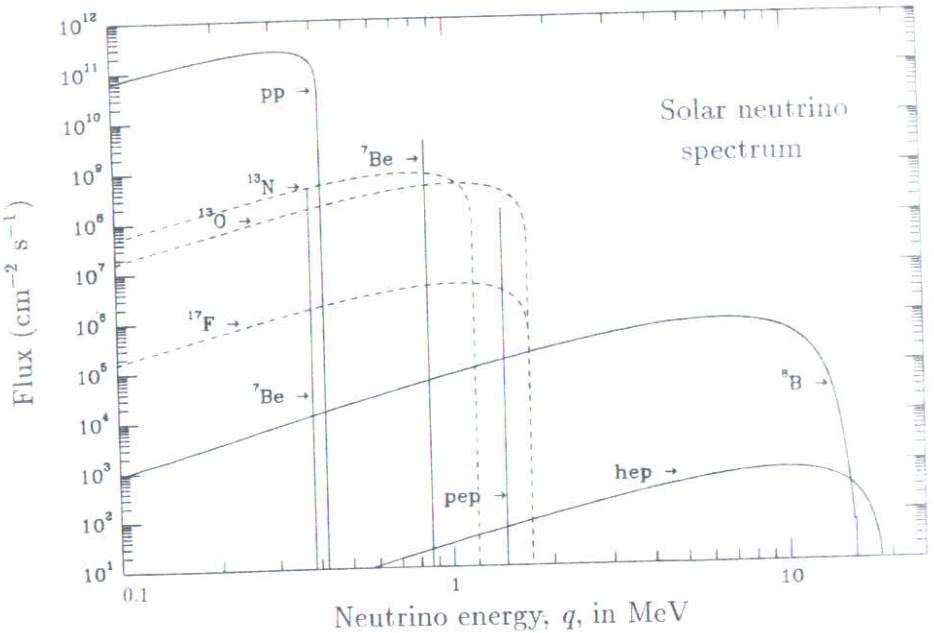

Figure 1.1 Solar neutrino spectrum This figure shows the energy spectrum of neutrinos predicted by the standard solar model. The neutrino fluxes from continuum sources (like pp and ^{8}B) are given in the units of number per cm^2 per second per MeV at one astronomical unit. The line fluxes (pep and ^{7}Be) are given in number per cm^2 per second. The spectra from the pp chain are drawn with solid lines; the CNO spectra are drawn with dotted lines. Chapter 6 discusses the neutrinos that are believed to be produced in the Sun.

$t_{atomic} \sim$ (random walk for a photon to escape from the center) $\approx 10^4\,yr$

$t_{nuclear} \sim \epsilon \times 0.1 \times M_\odot c^2/L_\odot \sim 10^{10}\,yr$

$\epsilon \approx 0.7\%$ (yield of $4p \rightarrow \alpha$)

da J. N. Bahcall (1989) Neutrino Astrophysics

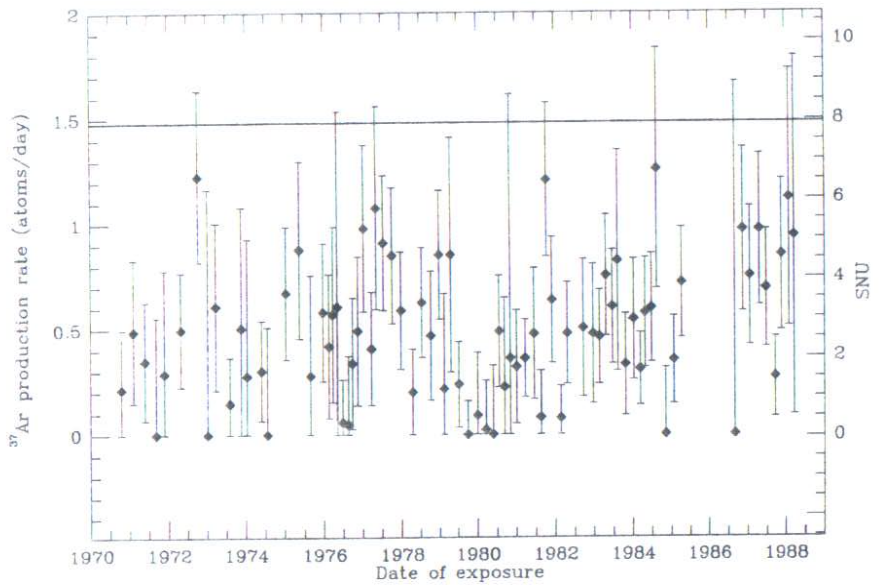

Figure 1.3 ^{37}Cl observations The observed rate in the ^{37}Cl solar neutrino experiment (from observations by Davis, Cleveland, and Rowley). The line at 7.9 SNU across the top of the figure represents the prediction of the standard model.

that is used for the detection of the neutrinos is:

$$\nu_e + {}^{37}\mathrm{Cl} \Rightarrow e^- + {}^{37}\mathrm{Ar}, \qquad (1.4)$$

Table 15.4. Measured properties of neutrino events from SN1987A observed in water Cerenkov detectors. The first events were detected on February 23, 1987 at about 7 hr 36 m UT. The angle in the last column is relative to the direction of the LMC. The errors are estimated 1σ uncertainties.

Event	Event time (s)	Electron energy (MeV)	Electron angle (degrees)
Kamiokande II:			
1	0	20.0 ± 2.9	18 ± 18
2	0.107	13.5 ± 3.2	40 ± 27
3	0.303	7.5 ± 2.0	108 ± 32
4	0.324	9.2 ± 2.7	70 ± 30
5	0.507	12.8 ± 2.9	135 ± 23
6	0.686	6.3 ± 1.7	68 ± 77
7	1.541	35.4 ± 8.0	32 ± 16
8	1.728	21.0 ± 4.2	30 ± 18
9	1.915	19.8 ± 3.2	38 ± 22
10	9.219	8.6 ± 2.7	122 ± 30
11	10.433	13.0 ± 2.6	49 ± 26
12	12.439	8.9 ± 1.9	91 ± 39
IMB:			
1	0	38 ± 7	80 ± 10
2	0.412	37 ± 7	44 ± 15
3	0.650	28 ± 6	56 ± 20
4	1.141	39 ± 7	65 ± 20
5	1.562	36 ± 9	33 ± 15
6	2.684	36 ± 6	52 ± 10
7	5.010	19 ± 5	42 ± 20
8	5.582	22 ± 5	104 ± 20

Il vento solare: scienziati russi ...; A. Bonetti ... B. Rossi (1963)

(16

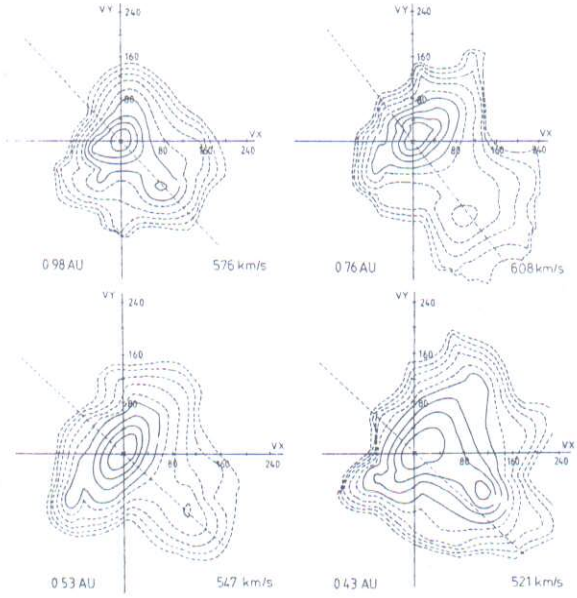

Figure 1. Isodensity contour plot of very non-thermal proton velocity distributions measured by Helios 2 in high speed solar wind at various heliocentric distances.

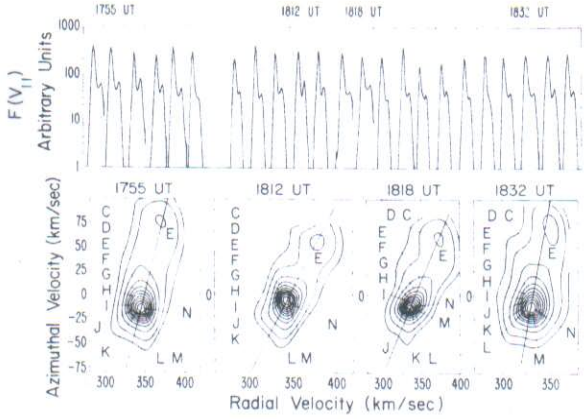

Figure 2. Double-humped proton distributions, plotted as one-dimensional spectra (top) and as contours (bottom), for a period with large temperature anisotropies and heat fluxes observed by IMP 6 on May 13 in 1971 (Ref. 1).

E. Marsch ESA SP-207 (1984)

WHAT are galaxies? No one knew before 1900. Very few people knew in 1920. All astronomers knew after 1924.

Galaxies are the largest single aggregates of stars in the universe. They are to astronomy what atoms are to physics. Each galaxy is a stellar system somewhat like our Milky Way, and isolated from its neighbors by nearly empty space. In popular terms, each galaxy is a separate "island universe" unto itself. The average density of matter in a galaxy is only 10^{-23} gram for every cubic centimeter. If this matter were spread over all of space in a uniform way, a density of only 10^{-30} to 10^{-31} g/cm^3 would result. Less than one-millionth of the total volume of the universe is occupied by condensations of matter.

It is almost certain that individual galaxies have not always been what they are today. We see the universe some 10 billion years after its last creation, but clues to its initial conditions remain. There has not been sufficient time for them to be obliterated, and if the proper observations are made and are properly interpreted, we can hope to reconstruct a history of its evolution. This hope drives cosmologists to think, causes large telescopes to be built, and makes observers work on cold winter nights. The hope is not vain. We do stand a chance of understanding the universe. And the present generation, with its great telescopes and its physical theories, may catch glimpses of the early stages of time.

A renaissance is occurring today in astronomy. It began in the 1920's, when physicists and theoretical astronomers asked, "What are the stars?" The theory of the stellar interior was developed by Eddington, his predecessors, his contemporaries, and his followers. The essence of the theory was published in one of the most important books ever written, Eddington's *Internal Constitution of the Stars*. This work opened the way for modern theories of stellar evolution—a field that is now in its infancy but which promises to consolidate many of the isolated facts in astronomy.

The theory of stellar structure combines the small-scale phenomena of the atoms with the intermediate-scale phenomena of the stars. But during the 1920's science was also advancing in cosmology, which has as its scope the largest-scale phenomena possible to observe—those of the universe itself. We are now at the crossroads. Insights deriving from the theory of stellar evolution are being applied to cosmological data from the universe at large. Out of the combination we now have a reasonable account of the formation of the elements, the beginnings of a theory for the evolution of galaxies themselves, and explanations for the presence or absence of all components of the stellar contents of galaxies. There is an exciting time ahead, limited only by the size of the telescopes and the ingenuity of the workers. This first chapter of the Hubble Atlas sketches cosmological thinking in the field of galaxies and the major change in it that took place in 1920. Some of the problems that lie in the immediate future for which there is good hope of a solution are then suggested.

Faint, nebulous objects with a discernible surface area have been known in the sky since the invention of the telescope. Speculation as to their nature was not confined to astronomers, but such men as Immanuel Kant (1724–1804), Emanuel Swedenborg (1688–1772), and Thomas Wright (1711–1786)

From "The Hubble Atlas of Galaxies"
Allan Sandage
1961 - Publication 618 - Carnegie Institution of Washington

to the large, neighboring spiral, M33. The two brightest of the objects discovered by Duncan were identified as irregular variables, and the faintest, as a Cepheid. By the

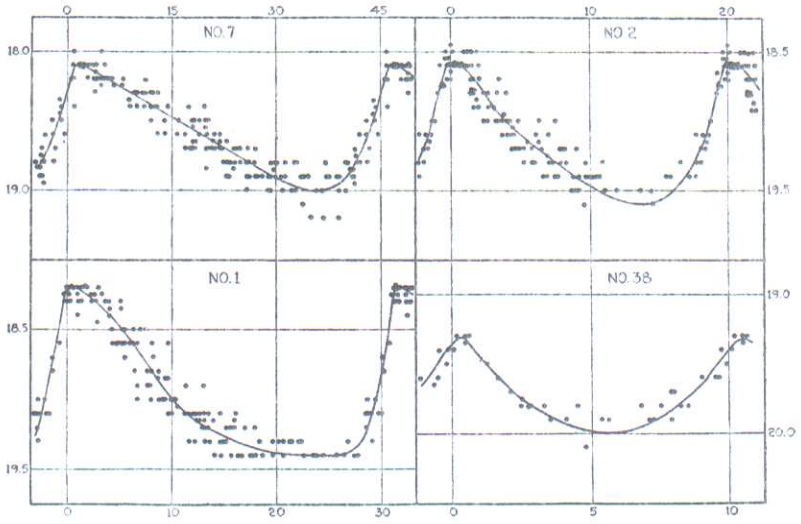

FIG. 8. *Light-Curves of Four Cepheids in Messier 31.*

The vertical scales represent apparent photographic magnitudes; the horizontal, days. The dots represent observations made during many different cycles. The various cycles were superposed and *normal* light-curves drawn through the totality of the data. It will be noticed that the brightest Cepheid, No. 7, has the longest period, and the faintest, No. 38, has the shortest period.

(18)

From: "The Realm of the Nebulae"
E. Hubble, 1936

(H. Shapley, revised by P. Hodge; Harvard U.P. 1971)

M 31 Pop.I, metal rich, Polaris

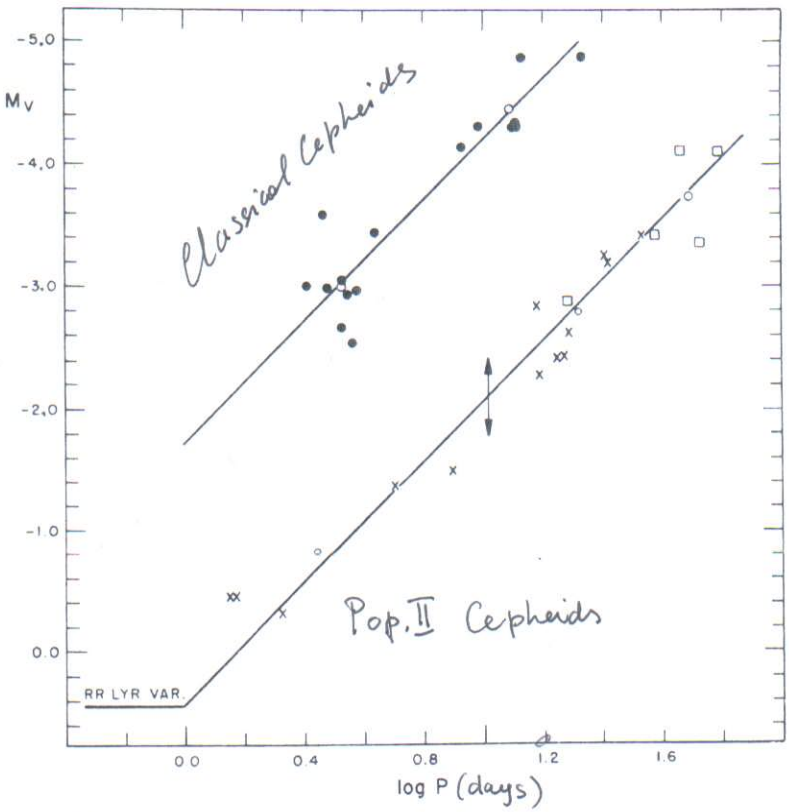

(g.c.)

Fig. 67. The period-luminosity relation for variable stars in an out-lying region of Messier 31. The upper curve is for the normal cepheid variables, and the lower curve is for the Population II cepheids. (From Baade and Swope, *Astronomical Journal.*)

SCALES

$M \sim 10^9 - 10^{12} M_\odot$ $(1 M_\odot \sim 2\times10^{33}\,g)$

$L \sim 1 - 100$ kpc $(1\,kpc \sim 3\times10^{21}\,cm)$

T

$t_{dyn} \sim 10^8 - 10^9$ yrs

$t_{Hubble} \sim 10^{10}$ yrs

$\tau_{**} \sim 10^{11} - 10^{12}$ yrs star-star relaxation

$\tau_{gas} \sim 10^7$ yrs cloud-cloud collisions

Milky Way (Our Galaxy)

$M \sim 2\times10^{11} M_\odot$ $\sigma_\odot \sim 50\, M_\odot/pc^2$ *
$\rho_\odot \sim 0.1\, M_\odot/pc^3$

$R_\odot \sim 8$ kpc distance of the Sun from galactic center

$V_{rot} \sim 220$ km/sec

$T_\odot \sim 200\times10^6$ yrs $\frac{t_{Hubble}}{T_\odot} \approx 60$ *

$\varepsilon_B \sim \varepsilon_{cr} \sim \varepsilon_{BB} \sim 1\,eV/cm^3$; $\frac{1}{2}\rho V^2 \sim 1\,keV/cm^3$

TABLE 3.2

Properties of Galactic Classical Cepheids*

Property	Range	
	From	To
Period (II)	1^d	50^d
Mean Luminosity (L)	300 $L_\odot$	26,000 $L_\odot$
Median Spectral Type	F5	G5
Mean Radius (R)	14 $R_\odot$	200 $R_\odot$
Mass (M)	$\lesssim$3.7 $M_\odot$	$\lesssim$14 $M_\odot$

*Subscript ⊙ denotes solar values.

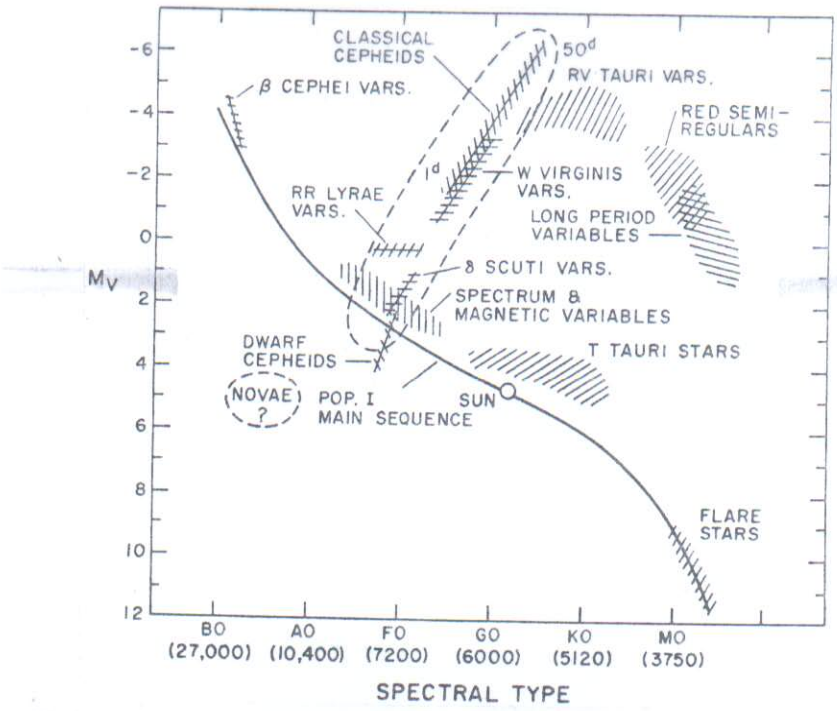

Figure 3.1. Location of a number of various types of intrinsic variables on the Hertzsprung-Russell diagram. From Figure 1 of J. P. Cox (1974a), courtesy of the Institute of Physics.

TABLE 3.1

The Pulsating Variables*

Kind of Star	Range of Periods	Characteristic Period	Population Type	Range of Spectral Types	Absolute Magnitude (M_V)
RR Lyrae	1.5–24 h	0.5 d	II	A2–F2	0.0 to +1.0
Classical Cepheids	1–50 d	5–10 d	I	F6–K2	−0.5 to −6
W Virginis Stars	2–45 d	12–20 d	II	F2–G6(?)	0 to −3
RV Tauri Stars	20–150 d	75 d	II	G, K	~−3
Red Semi-Regular Variables	100–200 d	100 d	I and II	(K), M, R, N, S	−1 to −3
Long Period Variables	100–700 d	270 d	I and II	M_e, R_e, N_e, S_e	+1 to −2
β Cephei Stars ("β Canis Majoris Stars")	4–6 h	5 h	I	B1–B2	−3.5 to −4.5
Dwarf Cepheids and δ Scuti Stars	1–3 h	2 h	I	A2–F5	+2 to +3
Beat Cepheids	1–7 d	2 d	I(?)	F0–G0(?)	−1 to −3(?)
Variable White Dwarfs ("ZZ Ceti Stars")	200–1000 s	500 s(?)	I(?)	A5–F5(?)	+10 to +15(?)

*Adapted from Table 1 of Cox (1974a), courtesy of the Institute of Physics.

("Theory of stellar pulsation" J.P. Cox 1980)

$m_\odot = -26.82$ $M_\odot = 4.75$ $L_\odot = 3.8 \times 10^{33}$ erg/s

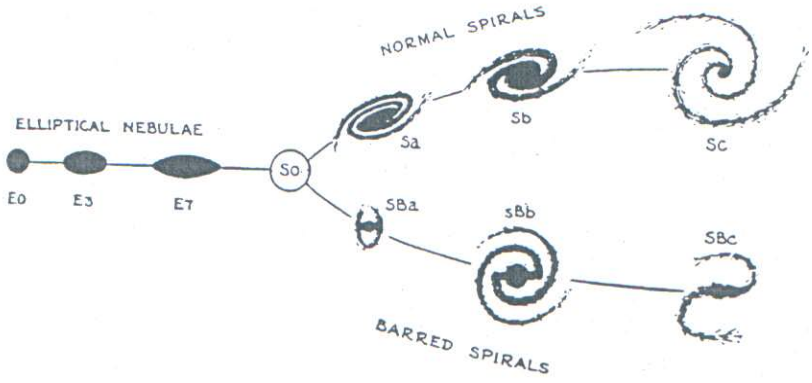

Figure 1.1
Hubble tuning fork diagram [11].

E. Hubble 1926 Astrophys. J.

Table 1.1
Hubble spiral sequences

$a \longrightarrow b \longrightarrow c$	
Gas content	Increasing
Size of HII regions	Increasing
Arm spacing	Increasing
Size of nuclear bulge	Decreasing
Total mass	Decreasing

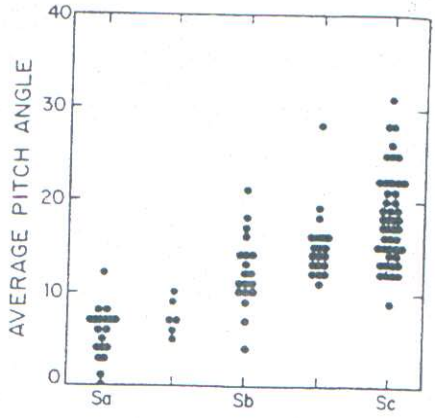

Figure 1.5
Measured pitch angle of spiral arms versus Hubble type [12].

R. C. Kennicutt 1981 Astron. J.

K-band (2μ)

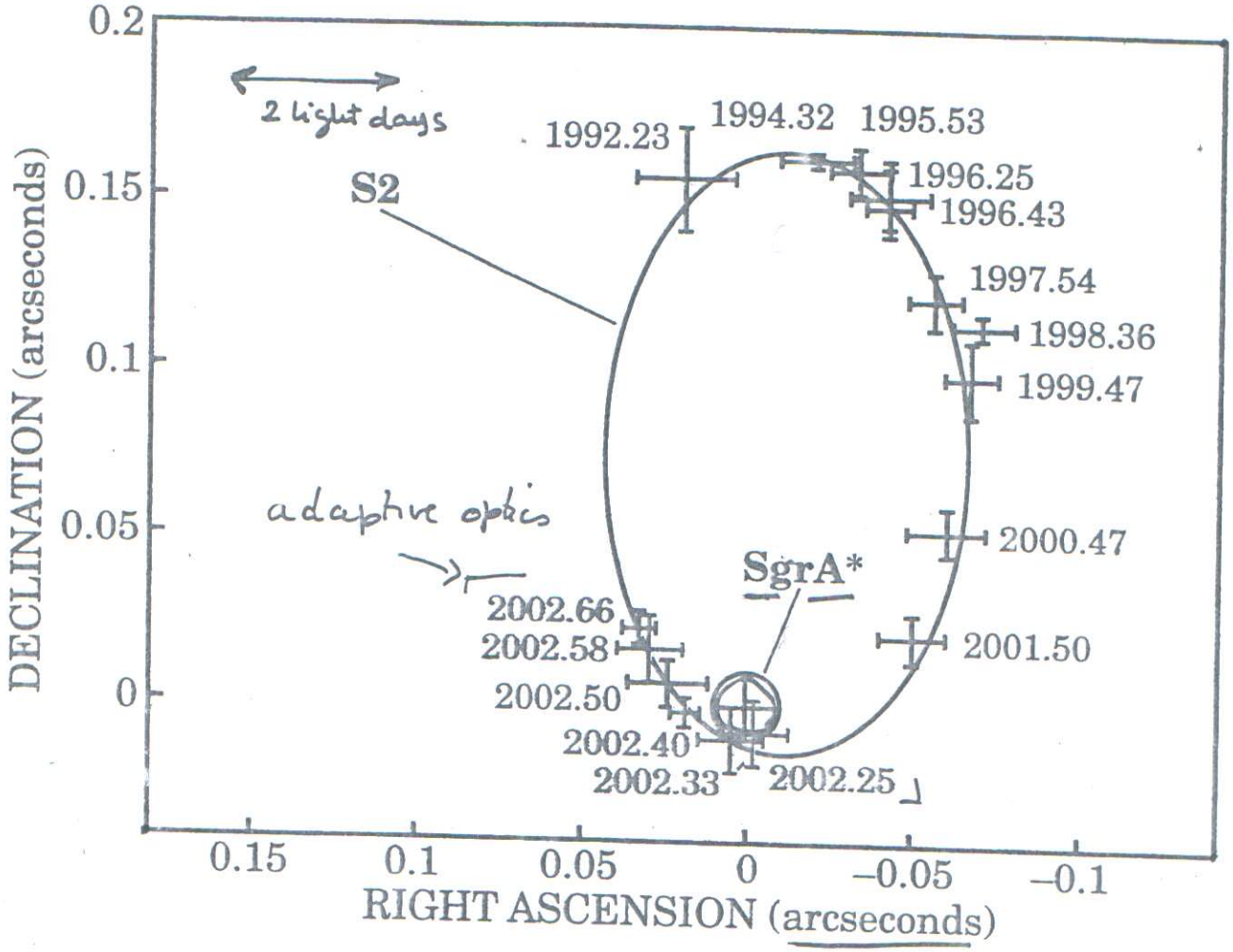

The positions of the star S2, circling the Galactic center with a period of only 15.2 years, are shown for 16 observations made by Rainer Schödel and colleagues, from March 1992 to July 2002. The blue crosses indicate adaptive-optics imaging. The ellipse is the best Keplerian fit to these observations and the measured position (the red circle) of the radio source Sgr A*, presumed to be a supermassive black hole at the Galactic center. The fitted orbit, inclined 46° to the line of sight, has S2 approaching to within 17 light-hours of the black hole.

15 $M_\odot$

$3.7 \pm 1.5 \times 10^6 M_\odot$

$\rightarrow 2.6 \pm 0.2 \times 10^6 M_\odot$

5000 km/s

Nature 419, 694 (2002)

Phys. Today Feb. 2003

(2)

DISCO DELLA GALASSIA VISTO DI TAGLIO

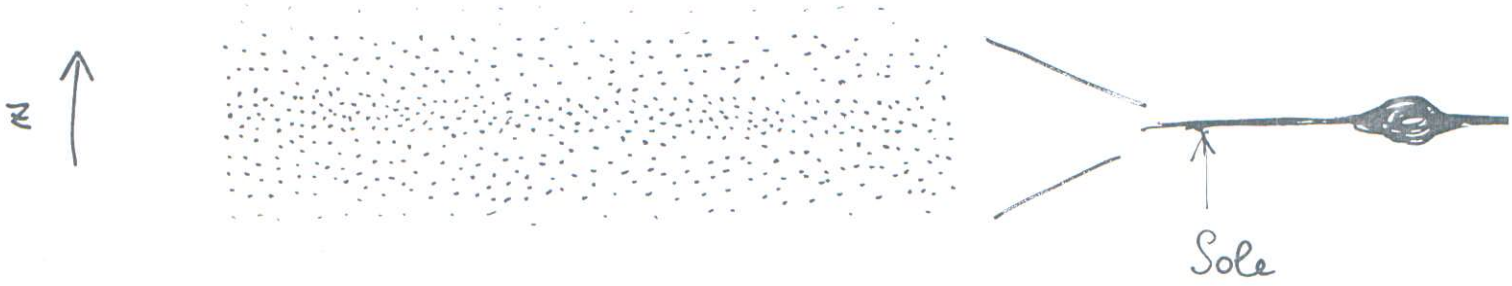

Componente verticale della velocità

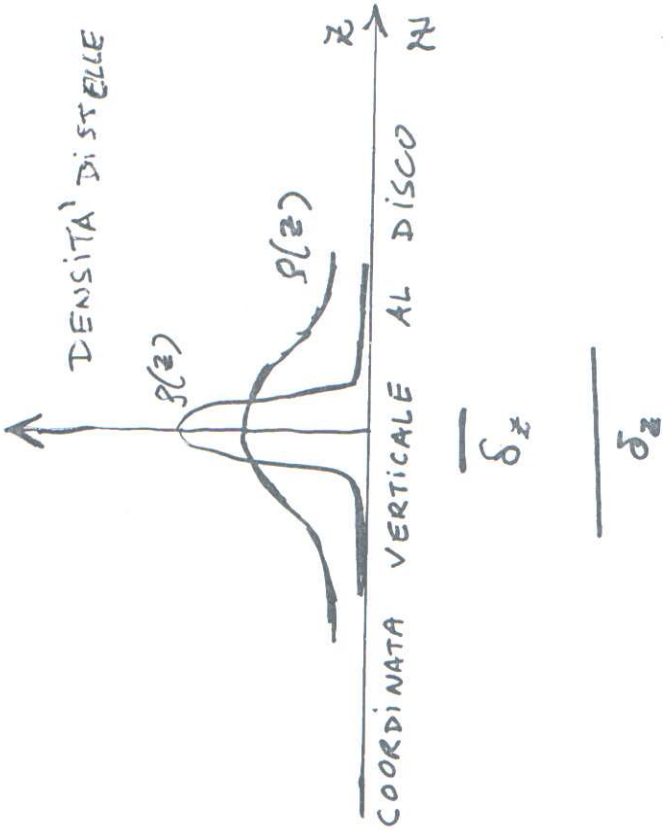

$$\delta \cdot (2\pi G \sigma) \approx c_z^2$$

$2h$ $\quad g \quad$ v^2

$$\cancel{m} g \cancel{h} = \frac{1}{2} \cancel{m} v^2$$

→ Oort 1932